

Site-Selective Excitation of Ti^{3+} Ions in Rutile TiO_2 via Anisotropic Intra-Atomic $3d \rightarrow 3d$ Transition

Jialong Li,[⊥] Tianjun Wang,[⊥] Shucaì Xia, Wei Chen, Zefeng Ren, Min Sun, Li Che,* Xueming Yang, and Chuanyao Zhou*



Cite This: *JACS Au* 2024, 4, 491–501



Read Online

ACCESS |

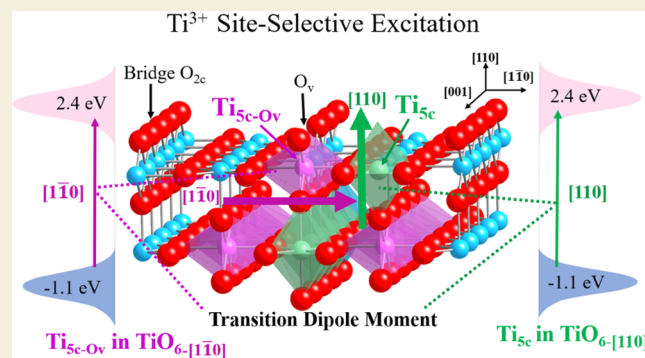
Metrics & More

Article Recommendations

Supporting Information

ABSTRACT: Site-selective excitation (SSE), which is usually realized by tuning the wavelength of absorbed light, is an ideal way to study bond-selective chemistry, analyze the crystal structure, investigate protein conformation, etc., eventually leading to active manipulation of desired processes. Herein, SSE has been explored in (110)-, (100)-, and (011)-faced rutile TiO_2 , a prototypical material in both surface science and photocatalysis fields. Using ultraviolet photoelectron spectroscopy and photon energy-, substrate orientation-, and laser polarization-dependent two-photon photoemission spectroscopy (2PPE), intra-atomic $3d \rightarrow 3d$ transition from the split Ti^{3+} 3d orbitals, i.e., band gap states and excited states at ~ 1.00 eV below and ~ 2.40 eV above the Fermi level, respectively, has been proven for all of the samples, suggesting that it is a common property of this material. The distinct structure of rutile TiO_2 results in the anisotropic $3d \rightarrow 3d$ transitions with the transition dipole moment along the long axes ($[110]$ and $[\bar{1}\bar{1}0]$) of TiO_6 blocking units. This anisotropy facilitates the selective excitation of Ti^{3+} ions in the two types of TiO_6 , which cannot be realized by conventional wavelength tuning, via polarization alignment of the excitation source. Discovery in this work builds the foundation for future investigation of site-selective photophysical and photochemical processes and eventually possible active manipulation in this material at the atomic level.

KEYWORDS: site-selective excitation (SSE), rutile TiO_2 , anisotropic intra-atomic $d \rightarrow d$ transition, atom-specific photophysics and photochemistry, two-photon photoemission spectroscopy (2PPE)



1. INTRODUCTION

Similar to state-selective excitation in molecules,^{1,2} quantum materials,^{3,4} and bulk materials⁵ through frequency tuning, site-selective excitation (SSE) can also be realized by making use of the characteristic absorption at distinct local environment sites and functional groups of materials. SSE can be used in unimolecular reactions to regulate the dynamics⁶ and in doped crystals to analyze the structure and manipulate the emission spectra.^{7–9} For proteins and biological membranes, SSE provides an additional dimension in fluorescence spectroscopy to study structures, dynamics, and interactions.^{10–12} In photosynthesis materials, excitation takes place at photosensitizer sites and charges transfer to catalytic active sites to initiate reactions.^{13–15} Sometimes, the roles of these two kinds of sites can be reversed, providing a chance to manipulate reactions.¹³

Semiconductor-based photocatalysis can convert solar energy to chemical fuels, holding hope in addressing energy and environmental issues.¹⁶ Titanium dioxide (TiO_2) is a model material in this field because of its relatively high photoactivity, affordability, nontoxicity, and photostability.^{17–28} Substrate atoms connect adsorbed atoms/mole-

cules/clusters via direct chemical bond formation, playing crucial roles in charge and energy transfer for subsequent surface physics and chemistry.²⁹ In-plane titanium and oxygen vacancy sites on TiO_2 surfaces are preferential locations for adsorbates because there are undercoordinated Ti atoms.²⁵ If these adsorption-related surface atoms can be selectively excited, driving force can be provided in the nearest proximity of target adsorbates to trigger desired surface physical and chemical processes and eventually realize active manipulation, as in the field of coherent control.³⁰

Rutile, the most stable crystallography of TiO_2 , is composed of vertex-connected TiO_6 octahedra with the long axes along $[110]$ and $[\bar{1}\bar{1}0]$ directions (Figure 1a),¹⁹ which will be denoted as $\text{TiO}_6\text{-}[110]$ and $\text{TiO}_6\text{-}[\bar{1}\bar{1}0]$, respectively, in the following text. On the most intensively studied (110) surface

Received: October 5, 2023
Revised: December 6, 2023
Accepted: January 3, 2024
Published: January 17, 2024



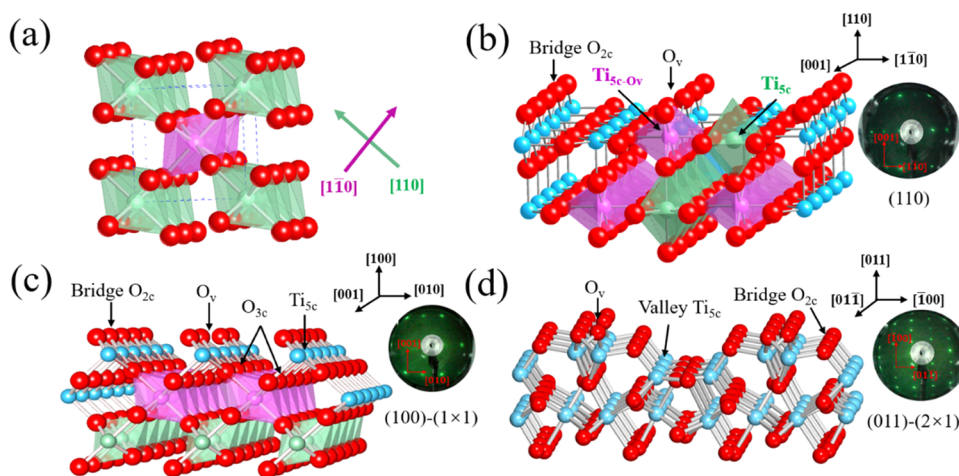


Figure 1. (a) Structure of rutile TiO_2 . Blue and red spheres represent titanium and oxygen atoms, respectively. The TiO_6 octahedron blocking units, i.e., $\text{TiO}_{6-[110]}$'s and $\text{TiO}_{6-[1\bar{1}0]}$'s, are highlighted in light green and purple, respectively. (b–d) The atomic structures of rutile $\text{TiO}_2(110)-(1 \times 1)$, $\text{TiO}_2(100)-(1 \times 1)$, and $\text{TiO}_2(011)-(2 \times 1)$ with their corresponding LEED images, respectively. Highly symmetric directions of the three TiO_2 surfaces are labeled by arrows. 2- and 3-fold coordinated oxygen (O_{2c} and O_{3c}), 5-fold coordinated Ti (Ti_{5c}), and oxygen vacancies (O_v) are indicated. Specially, on $\text{TiO}_2(110)$, surface $\text{TiO}_{6-[110]}$ and $\text{TiO}_{6-[1\bar{1}0]}$ and the corresponding Ti_{5c} and $\text{Ti}_{5c-\text{ov}}$ are labeled.

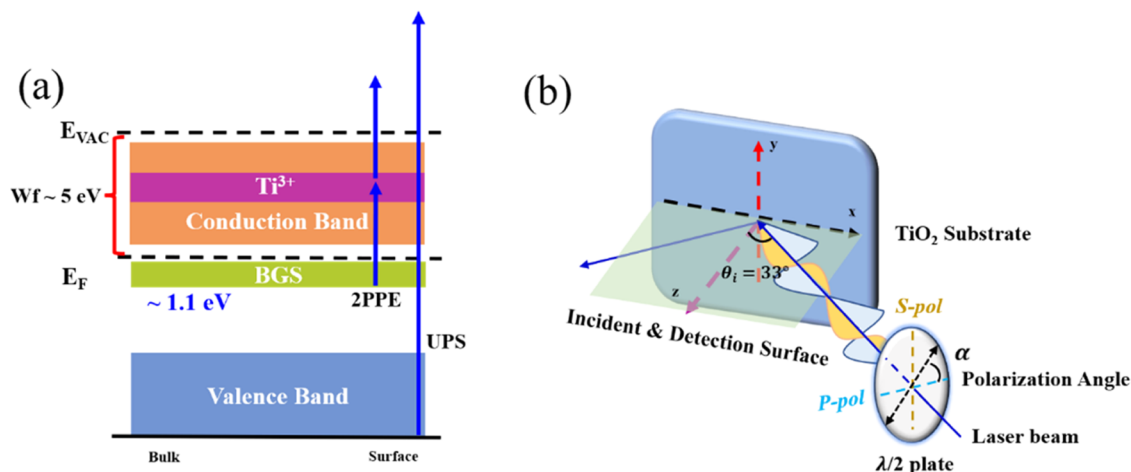


Figure 2. (a) Schematic diagram of 2PPE and UPS from TiO_2 . In 2PPE, an unequilibrated electronic structure is prepared by the “pump” pulse, occupying the empty states, which are then ionized by the “probe” pulse. It is worth noting that (1) the two-photon excitation starts from the BGS in the present work and (2) the probing depths of 2PPE and UPS are different (see main text for detail). (b) Configuration of the 2PPE experiments. The incident and detection planes coincide (light green plane, horizontal in the lab coordinates). The polarization angle α is defined as the angle between the electric field of the laser beam and the horizontal plane. P-pol/S-pol stands for the P-/S-polarized light, which means the electric field is parallel/perpendicular to the incident plane.

(Figure 1b), there are two types, namely, the in-plane (Ti_{5c}) and oxygen vacancy-related ($\text{Ti}_{5c-\text{ov}}$) 5-fold coordinated Ti ions, which are located at the center of $\text{TiO}_{6-[110]}$ and $\text{TiO}_{6-[1\bar{1}0]}$, respectively. The electronic structure of Ti ions near the Fermi level (E_F) is closely related to defects.^{31,32} Point defects such as oxygen vacancies,³¹ Ti interstitials,³³ and surface hydroxyls³⁴ can be readily introduced to rutile TiO_2 . The excess electrons brought by the defects disperse over several Ti sites, resulting in the partial reduction of center Ti ions in TiO_6 blocking units.^{35,36} For simplicity, these partially reduced Ti ions will be referred to as Ti^{3+} . The reduction is accompanied by the formation of localized polaronic band gap states (BGS) at about 1 eV below the E_F (Figure 2a).³¹ BGS are of mainly Ti^{3+} 3d character, which belongs to the t_{2g} orbitals in the distorted TiO_6 crystal field.³⁷ The roles of Ti^{3+} defects in photoabsorption,^{32,38–41} chemical adsorption,^{42–44} and surface chemistry^{45–47} have been frequently reported. Ti_{5c}

and $\text{Ti}_{5c-\text{ov}}$ on the $\text{TiO}_2(110)$ surface are two distinct adsorption sites where the surface chemistry is significantly different.²⁵ It is very intriguing to know whether these two types of Ti^{3+} ions can be selectively excited to serve the following physics and chemistry.

The ground states of Ti^{3+} in TiO_2 have been well characterized.^{31,33,34,36,48} Then, understanding the properties of Ti^{3+} -related excited states and the transition from ground to excited states is a prerequisite to address the above concern. Excited states at 2.40 ± 0.30 eV above the E_F of $\text{TiO}_2(110)$ have been detected by two-photon photoemission spectroscopy (2PPE; Figure 2a) for a long time, but the assignment of orbitals and the related transition are in debate. Petek et al. ascribed the excited states to e_g states of TiO_6 octahedra and proposed that there were two types of $3d \rightarrow 3d$ transitions in rutile TiO_2 : one was isotropic and the transition dipole moment of the other was along $[110]$.^{49,50} The conclusions on

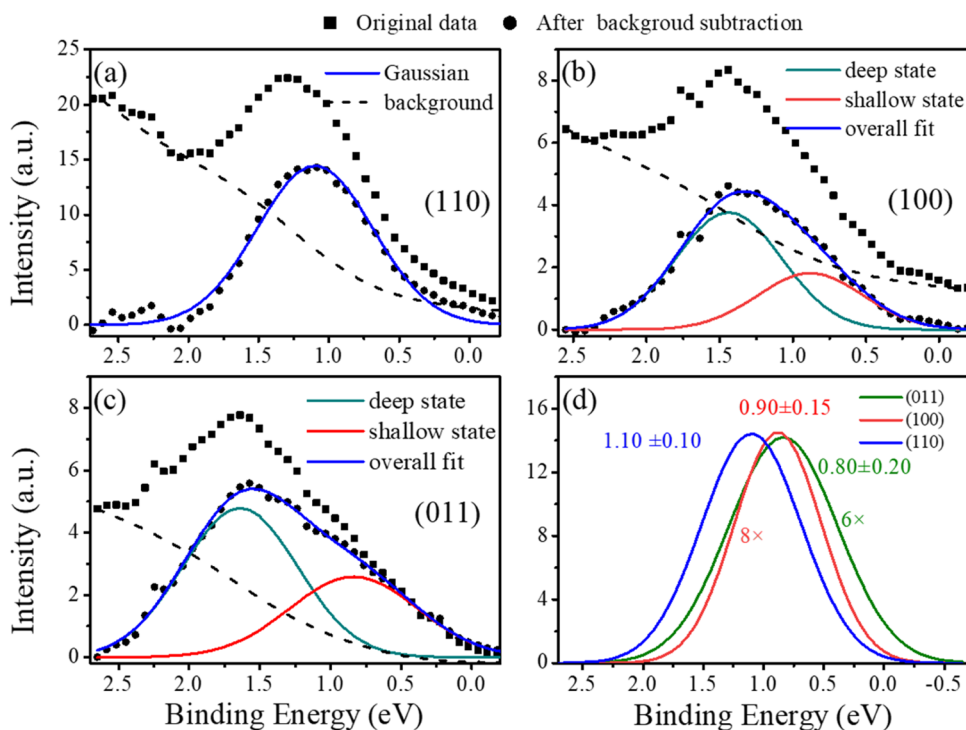


Figure 3. UPS spectra in the 2.5 to -0.5 eV binding energy range showing the band gap states of rutile TiO_2 (a) (110), (b) (100), and (c) (011). The data points were fitted by Gaussian functions after background (dashed lines) subtraction. The fitted curves were rescaled in (d) for a better comparison. The multiplied factors and center energies were specified.

the transition are inconsistent with the symmetry of rutile TiO_2 , which is composed of elongated TiO_6 - $_{[110]}$ and TiO_6 - $_{[\bar{1}\bar{1}0]}$. Thornton et al. suggested that the excited states were the unoccupied orbitals of surface hydroxyls.⁵¹ This attribution, however, is problematic because these states still exist without surface hydroxyls. By combining 2PPE measurements and density functional theory (DFT) calculations on TiO_2 (110), we have previously proposed that BGS and the excited states at 2.4 ± 0.3 eV above E_F originate from the splitting of t_{2g} orbitals in TiO_6 octahedra in the presence of the Jahn–Teller effect, and the resulting localized intra-atomic $3d \rightarrow 3d$ transitions are anisotropic with the transition dipole moments along the long axes of TiO_6 , i.e., $[110]$ and $[\bar{1}\bar{1}0]$.^{32,40}

So far, most of the discussion on $\text{Ti}^{3+} 3d \rightarrow 3d$ transition in rutile TiO_2 is limited to the (110) substrate. Though such transition has been mentioned in rutile TiO_2 (011), the existence of excited states has not been strictly proven.⁵² Whether the anisotropic $\text{Ti}^{3+} 3d \rightarrow 3d$ transition is a common feature in rutile TiO_2 and not subject to specific surface needs more evidence from other substrates besides (110). Therefore, systematic photon energy-, orientation-, and polarization-dependent 2PPE measurements are performed on rutile TiO_2 (110), (100), and (011) substrates. $\text{Ti}^{3+} 3d$ excited states at 2.4 ± 0.3 eV above E_F have been detected for all samples. Based on the hypothesis of anisotropic $\text{Ti}^{3+} 3d \rightarrow 3d$ transition along $[110]$ and $[\bar{1}\bar{1}0]$, the transition probabilities have been calculated within the dipole transition approximation as a function of substrate orientation and light polarization, which reproduce the experimental results fairly well. By proving the intrinsic anisotropic $\text{Ti}^{3+} 3d \rightarrow 3d$ transition in rutile TiO_2 , our work demonstrates that Ti^{3+} ions in rutile TiO_6 - $_{[110]}$ and TiO_6 - $_{[\bar{1}\bar{1}0]}$ can be selectively excited by light polarization alignment rather than conventional frequency tuning. The

finding paves the way for future investigation of site-selective photophysical and photochemical processes and eventually possible active manipulation in rutile TiO_2 , especially on the (110) surface where Ti_{5c} 's and $\text{Ti}_{5c\text{-ov}}$'s are exposed and are preferential adsorption sites showing distinct surface chemistry.

2. EXPERIMENTAL DETAILS

All experiments were performed in an ultrahigh vacuum (UHV) system (base pressure $< 5 \times 10^{-11}$ mbar) equipped with standard preparation and characterization devices such as an ion gun (IQE 11/35, SPECS), electron bombardment heating and liquid nitrogen cooling (100–1000 K) components, a low-energy electron diffractometer, and a hemispherical electron energy analyzer (Phoibos 100, SPECS).⁵³ The (110), (100), and (011) samples of rutile TiO_2 were prepared by cycles of Ar^+ sputtering (1 keV, 10 min) and annealing (30 min at 850, 670, and 850 K, respectively) until sharp low-energy electron diffraction (LEED) patterns were observed and contamination was below the detection limit of X-ray photoelectron spectroscopy (XPS). While the (110) and (011) samples were annealed in UHV, the (100) substrate was annealed in a 5×10^{-7} mbar oxygen atmosphere.⁵⁴ The resulting slightly reduced rutile TiO_2 (110), (100), and (011) samples exhibited well-ordered (1×1) , (1×1) , and (2×1) LEED patterns (Figure 1b–1d), respectively.

The randomly polarized He I ($h\nu = 21.2$ eV) from a helium lamp (UVS 10/35, SPECS) was chosen for the ultraviolet photoelectron spectroscopy (UPS) measurements. The second harmonic generation (SHG) of a Ti:sapphire oscillator (Mai Tai, Spectra-Physics) with a repetition rate of 80 MHz was utilized to realize the two-photon photoemission from TiO_2 . The photon energy of SHG in the ultraviolet region was tuned from 2.99 to 3.53 eV by varying the wavelength of the fundamental output of the oscillator before a BBO nonlinear crystal. The spot size, pulse energy, and pulse width of the exciting UV laser at the substrate surface were $\sim 100 \mu\text{m}$, 1.5 nJ, and ~ 100 fs, respectively.

The orientations of TiO_2 samples were varied by rotation around the surface normal (z -axis in Figure 2b), locating the highly symmetric directions of the substrate into the incident plane. The detection and

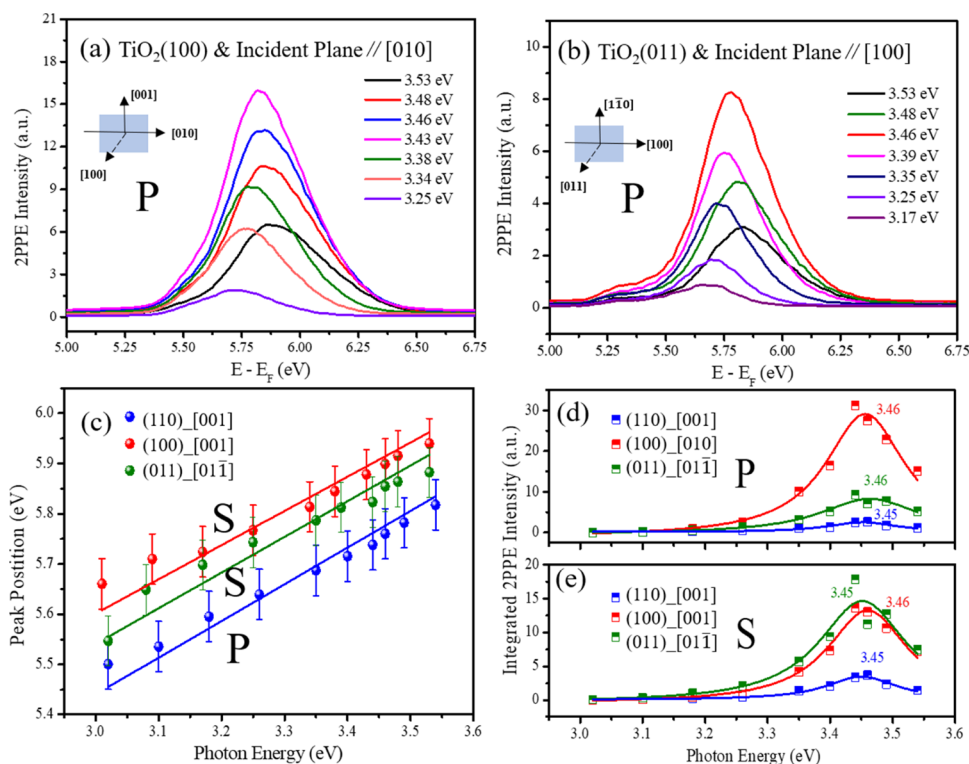


Figure 4. 2PPE spectra from rutile $\text{TiO}_2(100)$ (a) and (011) (b) as functions of photon energy. Experimental configurations are sketched in the inset pictures. (c) Peak positions of 2PPE spectra of rutile $\text{TiO}_2(110)$, (100) , and (011) as a function of photon energy and linear fitting. Dependence of the integrated (d) P-polarized (P) and (e) S-polarized (S) 2PPE signals of rutile $\text{TiO}_2(110)$, (100) , and (011) on the photon energy. The data points are obtained by normalizing the photon energy-dependent 2PPE intensity to the photon flux first and integrating the corresponding normalized 2PPE spectra after Henrich background subtraction. Solid lines are Lorentz fittings to the data points. Resonant energies are indicated. The parentheses and square brackets in the legends in (c–e) refer to the substrate surface plane and the in-plane highly symmetric direction in the laser incident plane, respectively. Selected data sets are displayed in (c–e), and the rest are shown in Figures S8 and S10 in the SI.

the incident planes coincide. The incident angle of the UV laser beam was 33° , and the polarization was controlled by a half waveplate in front of the UHV chamber. Photoelectrons were collected normally with a collection angle from -5 to $+5^\circ$. All of the photoelectron spectra were recorded with a pass energy of 20 eV and a sample temperature of 100 K. The TiO_2 substrates were flashed to 600 K from time to time to remove background water adsorption.

3. RESULTS AND DISCUSSION

The band gap of rutile TiO_2 is 3.05 eV, the work function (W_f) of TiO_2 samples under investigation is higher than 5.0 eV (Figure 4), and the Fermi level of reduced rutile TiO_2 lies about 0.40 eV below the conduction band minimum (CBM).⁵⁵ These lead to an energy difference of ~ 7.65 eV between the valence band maximum (VBM) and the vacuum level (E_{vac}). With the photon energy (2.99–3.53 eV) in the current work, only electrons from the BGS can be excited above the E_{vac} through two-photon photoemission. That is to say, BGS are the initial states in the 2PPE measurements in the present work. The occupied BGS of rutile $\text{TiO}_2(110)$, (100) , and (011) are studied first using UPS, followed by the investigation of the empty states by 2PPE.

3.1. Band Gap States of Rutile $\text{TiO}_2(110)$, (100) , and (011)

Figure 3 displays the UPS spectra in the 2.5 to -0.5 eV binding energy range for (110) , (100) , and (011) samples. Since in the adjacent 3–2 eV region, contribution from the satellite line of He I ($h\nu = 23.1$ eV) cannot be neglected,⁵⁶ we have added such satellite background to a Henrich secondary electron background.⁵⁷ Detailed description of the background

subtraction method can be found in the Supporting Information (SI).

After background subtraction, we can see that only the BGS on (110) can be fitted by one single Gaussian function centered at 1.10 eV, while those on (011) and (100) are apparently asymmetric (Figure 3a–3c). Therefore, they are fitted with two Gaussians, yielding peak positions at 0.88/1.44 eV for (100) and 0.84/1.64 eV for (011) . Two BGS at 0.70 and 2.20 eV corresponding to Ti^{3+} and unknown species, respectively, have been detected for $\text{TiO}_2(011)$.⁵⁸ The binding energy of the shallow state in our work is close to the reported one, while that of the deep state differs by 0.56 eV. The exact reason for the discrepancy, however, is not immediately clear. The quality of TiO_2 samples and the preparation history are possible factors. In addition to the unidentified origin, the deep band gap states are beyond the access of 2PPE with the photon energy in the current work. Consequently, for (100) and (011) , only the shallow BGS will be discussed later.

The intensity and the center of the BGS are highly substrate-dependent (Figure 3d). The shallow BGS intensity for (100) and (011) amounts to only ~ 10 and 20%, respectively, of that for (110) . Even including the deep states, BGS intensity for (100) and (011) is still only ~ 20 and 50%, respectively. The centers of the BGS are 1.10, 0.90, and 0.80 eV for (110) , (100) , and (011) , respectively. The experimental error is 0.2 eV according to the standard deviation from measurements at different locations on the sample surfaces.

The probing depth of photoelectron spectroscopy is determined by the inelastic mean free path of the produced

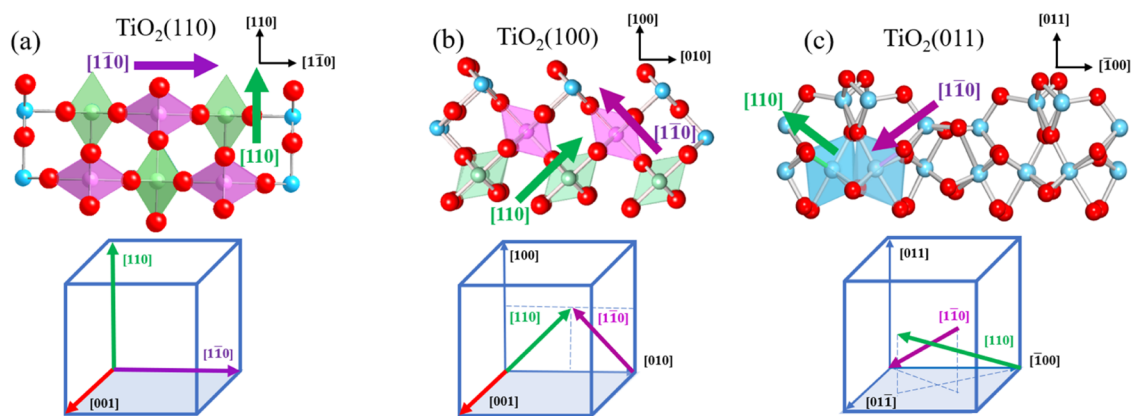


Figure 5. (Top) Front view of the geometric relation between the (a) (110), (b) (100), and (c) (011) surfaces, $\text{TiO}_{6-[\bar{1}10]}$ (light green) and $\text{TiO}_{6-[\bar{1}\bar{1}0]}$ (purple) octahedra and directions of Ti^{3+} 3d \rightarrow 3d transition dipole moment ($[110]$ (green) and $[\bar{1}\bar{1}0]$ (purple)) of rutile TiO_2 . Blue and red spheres represent titanium and oxygen atoms, respectively. Because of the reconstruction at the surface and subsurface of $\text{TiO}_2(011)$, TiO_6 octahedra are not standard $\text{TiO}_{6-[\bar{1}10]}$ and $\text{TiO}_{6-[\bar{1}\bar{1}0]}$. (Bottom) Cubic cells showing the surface (blue plane) and important directions of the three rutile TiO_2 substrates.

photoelectrons.⁵⁹ For UPS measurements with a photoelectron kinetic energy of several 10 eV (about 15 eV for the electrons from the BGS in the present work), the probing depth is only a few layers.⁶⁰ BGS of TiO_2 are associated with the Ti^{3+} caused by point defects such as oxygen vacancies, hydroxyls, and Ti interstitials.^{31,33,34,36} Therefore, the measured BGS intensity reflects the defect density in the topmost layers. It is not strange that the BGS intensity of (100) is much weaker than that of (110) because oxygen was used to prepare the former samples, resulting in the decrease of Ti^{3+} concentration within the probing depth of UPS. The relative BGS intensity of (011) and (110) is consistent with that under similar preparation procedures,⁶¹ suggesting that the formation energy of oxygen vacancies on the former surface is much higher than that on the latter one. The excess charges associated with the BGS of $\text{TiO}_2(100)$ are located deeper than those of $\text{TiO}_2(110)$.^{62,63} The preparation together with the intrinsic deeper location of the excess charges of $\text{TiO}_2(100)$ and $\text{TiO}_2(011)$ results in the difference in the probed UPS intensity compared with $\text{TiO}_2(110)$. The binding energies of BGS for $\text{TiO}_2(110)$ and shallow BGS for (100) and (011) fall into the reported energy range (0.60–1.30 eV).^{31,34,40,54,61,64}

3.2. Excited States of Rutile $\text{TiO}_2(110)$, (100), and (011)

Figure 4a,4b displays representative 2PPE spectra from rutile $\text{TiO}_2(100)$ and (011), respectively, as a function of exciting photon energy ($h\nu \sim 3.01\text{--}3.53$ eV) with selected experimental configurations (inset graphs). Those for $\text{TiO}_2(110)$ (Figure S5) and other configurations (Figures S6 and S7) are presented in the Supporting Information. These 2PPE spectra exhibit prominent intensities between 5.50 and 6.25 eV and shifting peak positions with photon energies. Owing to the “pump–probe” detection configuration of 2PPE, the spectra contain information of both initial and intermediate (if there are any) states. The slope (k) of the dependence of the final state energy (E_{final}) on the photon energy provides evidence for the origin of the 2PPE signals according to the following equations

$$E_{\text{final}} = E_{\text{initial}} + 2h\nu \quad (1)$$

$$E_{\text{final}} = E_{\text{intermediate}} + h\nu \quad (2)$$

where E_{initial} and $E_{\text{intermediate}}$ denote the initial and intermediate state energies, respectively. $k = 1$ (2) means that 2PPE signals come from the intermediate (initial) states.

The peak positions of the 2PPE spectra from $\text{TiO}_2(110)$, (100), and (011) substrates are plotted as a function of photon energy in Figure 4c. Linear fitting of the data points yields three almost parallel lines ($k = 0.71$). For $\text{TiO}_2(110)$, we have demonstrated that the 2PPE signals in this energy range arise from the empty Ti^{3+} 3d orbitals.^{32,40,52} The parallel dependence of the final state energy on the photon energy therefore suggests that there exist empty states at 2.4 ± 0.3 eV in rutile $\text{TiO}_2(100)$ and (011). The trend of the excited state levels is consistent with that of the BGS binding energy for these substrates, given the 0.2 eV experimental error. Similar to $\text{TiO}_2(110)$, the lifetime of the excited states in $\text{TiO}_2(100)$ and $\text{TiO}_2(011)$ are very short (less than 20 fs),^{32,49} and therefore, these electrons relax in the conduction band before ionization with 100 fs pulses, causing a peak position red shift in the high energy region and slopes in Figure 4c of less than 1 (a detailed explanation is included in the SI). Drawing analogy to rutile $\text{TiO}_2(110)$ and anatase $\text{TiO}_2(101)$,^{32,40,41,52} the 2PPE signals of rutile $\text{TiO}_2(100)$ and (011) can be attributed to the localized Ti^{3+} 3d \rightarrow 3d transition. That is to say, the Ti^{3+} 3d \rightarrow 3d transition is a common phenomenon in rutile TiO_2 .

In order to find the resonant energy of Ti^{3+} 3d \rightarrow 3d transition in rutile TiO_2 , the 2PPE signals of (110), (100), and (011) substrates are integrated after background subtraction and displayed versus photon energy (Figure 4d,e). Lorentz fitting to the data points yields resonant energies of 3.45/3.46 eV for all three substrates, which are consistent with the energy difference between BGS and excited states in this work and our previous measurements.^{40,52} The consistent resonant Ti^{3+} 3d \rightarrow 3d transition energies for all three substrates further indicate that it is a common feature of rutile TiO_2 .

Noteworthy, the 2PPE signals of the three TiO_2 substrates are comparable, though the UPS-measured BGS (initial states in 2PPE) intensity of (110) is much higher than those of (100) and (011). Because of the lower kinetic energy of photoelectrons in 2PPE compared with UPS in the present work, the probing depth of the former is larger than that of the latter.⁶⁰ Therefore, the different intensity ratio ((100) and (011) relative to (110)) of 2PPE and UPS suggests that Ti^{3+} defects

Table 1. Predicted Probability of the $\text{Ti}^{3+} 3d \rightarrow 3d$ Transition in Rutile TiO_2 as a Function of Substrate Surface, Substrate Orientation, and Laser Light Polarization^a

TiO ₂ surfaces	TiO ₂ orientation (direction in the incident plane)	transition probability						transition probability $P_{\text{TP}}/P_{\text{TS}}$	measured intensity $I_{\text{P}}/I_{\text{S}}$	relative discrepancy $\left \frac{P_{\text{TP}}/P_{\text{TS}} - I_{\text{P}}/I_{\text{S}}}{I_{\text{P}}/I_{\text{S}}} \right $
		P-pol		S-pol		possibility	possibility			
		electric field direction	possibility	electric field direction	possibility					
(110)	[001]	[110], [001]	A	[1 $\bar{1}$ 0]	A	0.29:1.00	0.29:0.58	0.42		
	[1 $\bar{1}$ 0]	[110], [1 $\bar{1}$ 0]	A	[001]	F	0.99:0	0.99:0.13			
(100)	[010]	[100], [010]	A	[001]	F	0.99:0	0.99:0.03	0.52		
	[001]	[100], [001]	A	[010]	A	0.29:1.00	0.29:0.48			
(011)	[$\bar{1}$ 00]	[011], [$\bar{1}$ 00]	A	[01 $\bar{1}$]	A	0.95:1.00	0.95:1.83	0.83		
	[01 $\bar{1}$]	[011], [01 $\bar{1}$]	A	[$\bar{1}$ 00]	A	0.84:0.50	0.84:0.43		0.14	

^aIn the third and fifth columns, the directions of the projected electric field of the exciting laser beam are indicated. A and F denote “allowed” and “forbidden,” respectively. Calculated transition probability ($P_{\text{TP}}/P_{\text{TS}}$) and measured intensity ($I_{\text{P}}/I_{\text{S}}$) ratio between P-2PPE and S-2PPE (measured by P- and S-polarized light, respectively), and the relative discrepancies are shown in the last three columns. Details of the calculations are included in the text and SI.

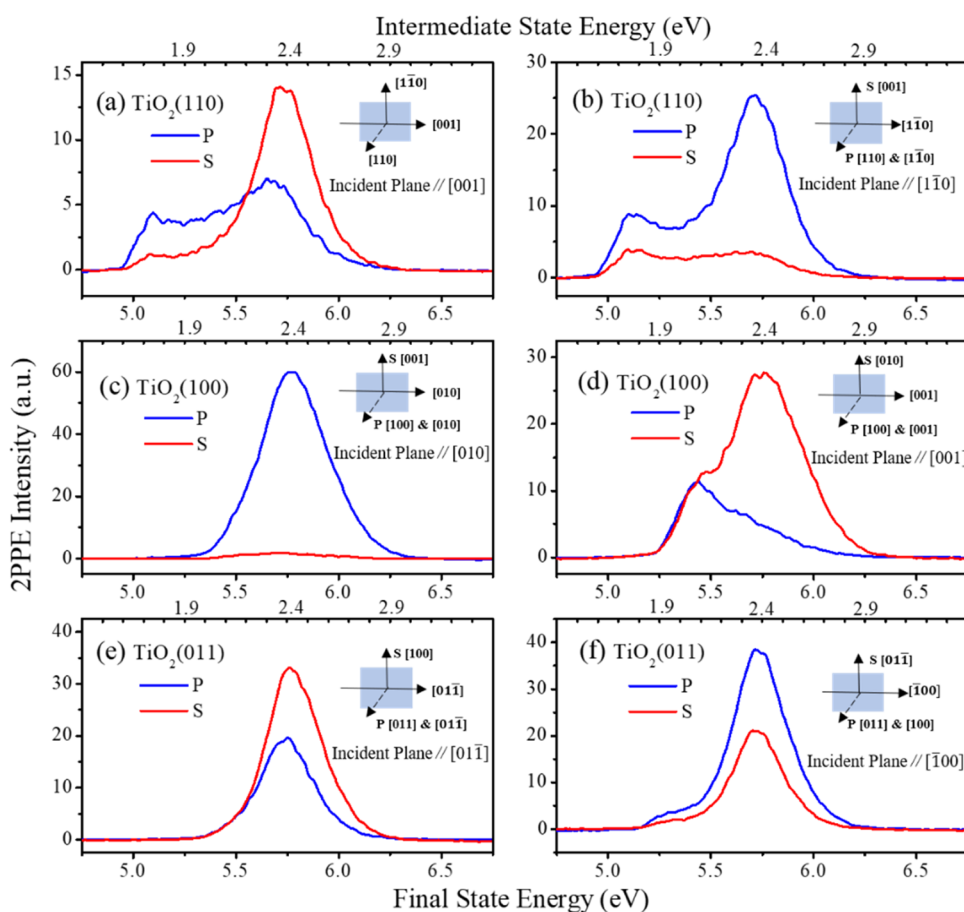


Figure 6. Rutile TiO_2 substrate surface-, substrate orientation-, and laser polarization-dependent 2PPE spectra acquired at a photon energy of 3.35 eV. The surfaces, orientations, and polarization are labeled. (a, b) $\text{TiO}_2(110)$ with the incident plane along (a) [001] and (b) [$\bar{1}$ 10]. (c, d) $\text{TiO}_2(100)$ with the incident plane along (c) [010] and (d) [001]. (e, f) $\text{TiO}_2(011)$ with the incident plane along (e) [01 $\bar{1}$] and (f) [$\bar{1}$ 00]. P and S represent the polarization of the laser beam used to acquire the 2PPE spectra.

in $\text{TiO}_2(100)$ and (011) are located deeper than those in $\text{TiO}_2(110)$, confirming previous studies.^{61,62}

3.3. Anisotropy of $3d \rightarrow 3d$ Transition in Rutile TiO_2

Now that $\text{Ti}^{3+} 3d \rightarrow 3d$ transition is an intrinsic property of rutile TiO_2 , what are the directions of the transition dipole moment? Rutile TiO_2 is composed of TiO_6 units with long axes of octahedra along [110] and [$\bar{1}$ 10].¹⁹ In previous work,

we proposed that the $3d \rightarrow 3d$ transition in rutile TiO_2 is anisotropic with the transition dipole moment along the long axes of TiO_6 blocking units based on the measurements from $\text{TiO}_2(110)$.^{40,52} To provide further support for this hypothesis, additional orientation- and polarization-dependent 2PPE measurements on other low-Miller-index-faced rutile TiO_2 substrates are necessary.

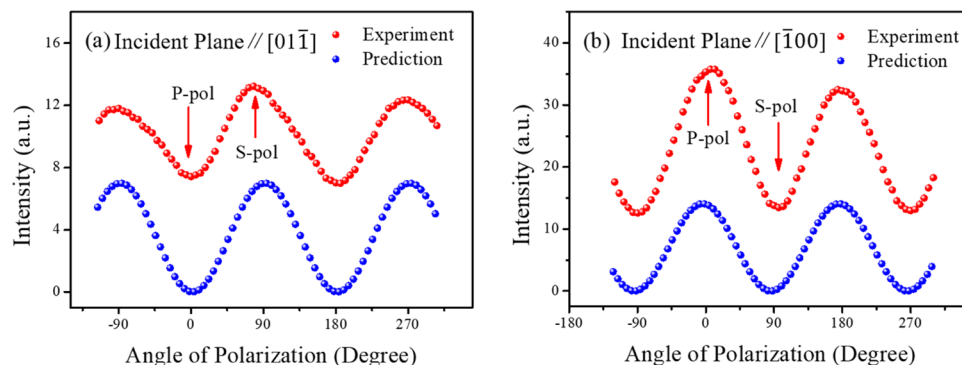


Figure 7. Polarization angle dependence of the calculated Ti^{3+} $3d \rightarrow 3d$ transition probability (blue spheres) and the measured 2PPE intensity (red spheres) in rutile $\text{TiO}_2(011)$ with the incident plane along (a) $[01\bar{1}]$ and (b) $[1\bar{0}0]$. The 2PPE intensities are obtained by integrating the background-free spectra.

Figure 5 shows the geometric relation between the (110), (100), and (011) surfaces and the $[110]$ and $[1\bar{1}0]$ directions of rutile TiO_2 . Aligning the in-plane highly symmetric directions with the incident plane, the directions of the projected electric field of the laser beam can be obtained (Table 1). In the dipole transition approximation, if there is an electric field projected along the direction of the transition dipole moment, a transition can take place. To simplify, when the electric field is along the $[001]$ direction, as indicated by red arrows in Figure 5a,5b, which is perpendicular to both $[110]$ and $[1\bar{1}0]$, the transition is forbidden. According to the above analysis, in the case of $\text{TiO}_2(110)$ and (100), $3d \rightarrow 3d$ transitions are forbidden under S-polarized light excitation if the $[1\bar{1}0]$ and $[010]$ planes are rotated into the incident plane respectively. In the rest of the configurations, $3d \rightarrow 3d$ transitions are allowed. The measured configuration-dependent 2PPE is qualitatively consistent with the prediction (Figure 6).

To be more quantitative, the Ti^{3+} $3d \rightarrow 3d$ transition probabilities are calculated for various experimental configurations under dipole transition approximation. There are three substrates, and each substrate has two highly symmetric directions on the surface, resulting in six experimental configurations. For each configuration, 2PPE spectra can be acquired with both P-polarized (P-2PPE) and S-polarized (S-2PPE) light. The transition dipole moment along $[110]$ and $[1\bar{1}0]$, i.e., $\vec{\mu}_{110}$ and $\vec{\mu}_{1\bar{1}0}$, respectively, are assumed to be the same, which is reasonable, since the two types of TiO_6 octahedra are equivalent in bulk rutile TiO_2 . Then, the transition dipole moment and the electric field of P-polarized (\vec{E}_p) and S-polarized (\vec{E}_s) light can be written as

$$\vec{\mu}_{110} = \left[\frac{1}{\sqrt{2}}, \frac{1}{\sqrt{2}}, 0 \right] \quad (3)$$

$$\vec{\mu}_{1\bar{1}0} = \left[\frac{1}{\sqrt{2}}, -\frac{1}{\sqrt{2}}, 0 \right] \quad (4)$$

$$\vec{\mu} = \vec{\mu}_{110} + \vec{\mu}_{1\bar{1}0} \quad (5)$$

$$\vec{E}_p = A \cos(\alpha) \cos(33^\circ) \vec{x} + A \cos(\alpha) \sin(33^\circ) \vec{z} \quad (6)$$

$$\vec{E}_s = A \sin(\alpha) \vec{y} \quad (7)$$

$$\vec{E} = \vec{E}_p + \vec{E}_s \quad (8)$$

where $\vec{\mu}$, \vec{E} , A , α , \vec{x} , \vec{y} , and \vec{z} stand for the total transition dipole moment, the total electric field, the amplitude of the electric field, the polarization angle relative to the incident plane, and the unit vectors along x , y , and z axes (Figure 2b), respectively. The square of the module of the dot product between the transition dipole moment and the electric field can be used to compare the transition probability (P_T).

$$P_{TP} \propto |\vec{\mu} \cdot \vec{E}_p|^2 \quad (9)$$

$$P_{TS} \propto |\vec{\mu} \cdot \vec{E}_s|^2 \quad (10)$$

Here, P_{TP} and P_{TS} are the transition probability under the excitation of P- and S-polarized light, respectively. The ratio between P_{TP} and P_{TS} can be calculated for each experimental configuration (details are included in the SI) and listed in Table 1.

To verify the predicted results, a series of substrate surface-, substrate orientation-, and laser polarization-dependent 2PPE experiments were conducted using a photon energy of 3.35 eV (Figure 6). Because of the substrate-dependent Ti^{3+} density and $3d \rightarrow 3d$ transition probability (distortion of TiO_6 octahedra), the intensities are compared and discussed for the same substrate rather than between different substrates. The ratios between the intensity of P-2PPE and S-2PPE (I_p/I_s) after Henrich background subtraction are listed in Table 1. The calculated P_{TP}/P_{TS} values are compared quantitatively with the measured I_p/I_s by normalizing I_p and the corresponding P_{TP} .

Overall, the predicted relative transition probabilities (P_{TP}/P_{TS}) agree well with measured I_p/I_s . Especially for the two experimental configurations where the transition is predicted to be forbidden under S-polarized light excitation, the measured I_p/I_s reaches 7.62:1 and 33:1, respectively. In other cases, the relative discrepancies between the calculated transition probability ratio and the measured intensity ratio ranged from 14 to 83%. The deviation likely comes from the simplification of the calculation, where the details of the wave functions of the initial (BGS) and intermediate (empty Ti^{3+} $3d$ around 2.4 ± 0.3 eV) states, the ionization cross section (which could be anisotropic) of the intermediate states, and contribution from Ti interstitials are not considered. Despite the exact values, these consistent intensity ratios suggest the rationality of the hypothesis of anisotropic Ti^{3+} $3d \rightarrow 3d$ transition in rutile TiO_2 .

Fixing the experimental configuration, the variation of the 2PPE intensity with the polarization of the exciting laser

provides another evidence for checking the direction of the transition dipole moment.^{40,52} According to the above analysis, the total transition probability can be written as follows.

$$P_T \propto |\vec{\mu} \cdot \vec{E}|^2 \quad (11)$$

$$P_{T_{01\bar{1}}} \propto |\vec{\mu} \cdot \vec{E}|^2 = |\sqrt{2}A \sin(\alpha)|^2 \quad (12)$$

$$P_{T_{100}} \propto |\vec{\mu} \cdot \vec{E}|^2 = |\sqrt{2}A \cos(\alpha)\cos(33^\circ)|^2 \quad (13)$$

For the more complicated $\text{TiO}_2(011)$, P_T is calculated as a function of α in both configurations (eqs 12 and 13 and Figure 7), i.e., the incident plane parallel to $[01\bar{1}]$ and $[\bar{1}00]$, respectively. When the incident plane is along $[01\bar{1}]$, the maximum/minimum intensity appears at $90/0^\circ$, while in the other configuration, the trend is totally antiphased. The polarization-dependent 2PPE is then recorded at corresponding configurations for comparison. The dependence of the calculated P_T on the polarization angle reproduces the measured 2PPE intensity well, confirming the correctness of the assumption of the $\text{Ti}^{3+} 3d \rightarrow 3d$ transition in rutile TiO_2 , i.e., the anisotropic transition along $[110]$ and $[\bar{1}\bar{1}0]$, which arises from the special structure of rutile TiO_2 .

Proving the intrinsic anisotropic $\text{Ti}^{3+} 3d \rightarrow 3d$ transition in rutile TiO_2 , we demonstrate that Ti^{3+} ions in $\text{TiO}_{6-[110]}$ and $\text{TiO}_{6-[\bar{1}\bar{1}0]}$ can be selectively excited by proper combination of the substrate surface, substrate orientation, and light polarization, rather than tuning the frequency of excitation light as researchers do in hybridized photocatalysts.¹³ Such SSE provides a new pathway to study atom-specific physical and chemical processes both in the bulk and at the surface of TiO_2 .

Especially TiO_2 is widely used in heterogeneous catalysis where the interfacial interaction plays critical roles. Adsorption can modify the interfacial properties significantly. On the one hand, adsorption on TiO_2 is reported to stabilize excess electrons at the surface,^{65–67} and the $d \rightarrow d$ transition can also get enhanced.^{56,68} On the other hand, adsorption leads to the hybridization of orbitals between the adsorbate and the substrate, facilitating interfacial electron transfer in 10 fs.^{69–71} Such a time scale is comparable with the lifetime of the $\text{Ti}^{3+} 3d$ states in TiO_2 .⁴⁹ Ti_{5c} and Ti_{5c-ov} , which are preferential adsorption sites of distinct properties on the $\text{TiO}_2(110)$ surface, can be selectively excited because they are at the center of $\text{TiO}_{6-[110]}$ and $\text{TiO}_{6-[\bar{1}\bar{1}0]}$, respectively. Enhanced $\text{Ti}^{3+} 3d \rightarrow 3d$ transition and orbital hybridization at the adsorbate/ $\text{TiO}_2(110)$ interface make it an ideal platform to study and manipulate desired electron transfer. The lifetime of adsorbed negative species is usually too short for the reaction to take place at the excited potential energy surface (PES).^{72,73} However, similar to the desorption induced by the electronic transition mechanism,⁷⁴ decay of the excited species back to the ground state after traveling on the excited PES can deposit vibrational energy to the adsorbates. Such a non-adiabatic energy coupling can provide the driving force for the following reactions.

CONCLUSIONS

In summary, through systematic UPS and photon energy-, substrate orientation- and laser polarization-dependent 2PPE measurements on (110), (100), and (011) substrates, splitting of $\text{Ti}^{3+} 3d$ orbitals in TiO_6 octahedra to BGS and excited states at 2.4 ± 0.3 eV above the E_F and the resulting intra-atomic $3d \rightarrow 3d$ transition have been proven to be common properties of rutile TiO_2 . Owing to the distinct structure of rutile TiO_2 , the

$3d \rightarrow 3d$ transition is anisotropic with the transition dipole moment along $[110]$ and $[\bar{1}\bar{1}0]$, which facilitates the selective excitation of Ti^{3+} ions in $\text{TiO}_{6-[110]}$ and $\text{TiO}_{6-[\bar{1}\bar{1}0]}$ by aligning the polarization of the excitation source rather than tuning the frequency. This result provides an avenue to realize site-selective physics and chemistry in this model material and eventually possible atom-specific control.

ASSOCIATED CONTENT

Supporting Information

The Supporting Information is available free of charge at <https://pubs.acs.org/doi/10.1021/jacsau.3c00600>.

Background subtraction for UPS; full data sets of excited states of rutile $\text{TiO}_2(110)$, (100), and (011); photon energy-dependent peak shift in 2PPE; resonant energy of $\text{Ti}^{3+} 3d \rightarrow 3d$ transition in rutile TiO_2 ; and calculation of the transition probability (PDF)

AUTHOR INFORMATION

Corresponding Authors

Li Che – Department of Physics, School of Science, Dalian Maritime University, 116026 Dalian, China; Phone: +86-411-84379701; Email: liche@dmlu.edu.cn; Fax: +86-411-84675584

Chuanyao Zhou – State Key Laboratory of Molecular Reaction Dynamics, Dalian Institute of Chemical Physics, Chinese Academy of Sciences, 116023 Dalian, China; University of Chinese Academy of Sciences, 100049 Beijing, China; orcid.org/0000-0002-3252-2992; Email: chuanyaozhou@dicp.ac.cn

Authors

Jialong Li – Department of Physics, School of Science, Dalian Maritime University, 116026 Dalian, China; State Key Laboratory of Molecular Reaction Dynamics, Dalian Institute of Chemical Physics, Chinese Academy of Sciences, 116023 Dalian, China

Tianjun Wang – State Key Laboratory of Molecular Reaction Dynamics, Dalian Institute of Chemical Physics, Chinese Academy of Sciences, 116023 Dalian, China

Shucui Xia – State Key Laboratory of Molecular Reaction Dynamics, Dalian Institute of Chemical Physics, Chinese Academy of Sciences, 116023 Dalian, China

Wei Chen – State Key Laboratory of Molecular Reaction Dynamics, Dalian Institute of Chemical Physics, Chinese Academy of Sciences, 116023 Dalian, China; University of Chinese Academy of Sciences, 100049 Beijing, China

Zefeng Ren – State Key Laboratory of Molecular Reaction Dynamics, Dalian Institute of Chemical Physics, Chinese Academy of Sciences, 116023 Dalian, China; orcid.org/0000-0002-5263-9346

Min Sun – Department of Physics, School of Science, Dalian Maritime University, 116026 Dalian, China

Xueming Yang – State Key Laboratory of Molecular Reaction Dynamics, Dalian Institute of Chemical Physics, Chinese Academy of Sciences, 116023 Dalian, China; Department of Chemistry, Southern University of Science and Technology, 518055 Shenzhen, Guangdong, China; orcid.org/0000-0001-6684-9187

Complete contact information is available at: <https://pubs.acs.org/doi/10.1021/jacsau.3c00600>

Author Contributions

[†]J.L. and T.W. contributed equally to this work. CRediT: **Jialong Li** data curation, formal analysis, investigation, writing-original draft; **Tianjun Wang** data curation, formal analysis, investigation, writing-review & editing; **Shucaï Xia** formal analysis; **Wei Chen** data curation; **Zefeng Ren** resources; **Min Sun** supervision; **Li Che** funding acquisition, supervision; **Xueming Yang** funding acquisition; **Chuanyao Zhou** conceptualization, formal analysis, funding acquisition, project administration, supervision, writing-review & editing.

Notes

The authors declare no competing financial interest.

ACKNOWLEDGMENTS

This work was financially supported by the National Key Research and Development Program of China (2021YFA1500601), the National Natural Science Foundation of China (22322306, 21973092, 22288201, and 21973010), the Chinese Academy of Sciences (YSBR-007), and the LiaoNing Revitalization Talents Program (XLYC1907032).

REFERENCES

- (1) Wang, T.; Chen, J.; Yang, T.; Xiao, C.; Sun, Z.; Huang, L.; Dai, D.; Yang, X.; Zhang, D. H. Dynamical Resonances Accessible Only by Reagent Vibrational Excitation in the F + HD → HF + D Reaction. *Science* **2013**, *342* (6165), 1499–1502.
- (2) Chang, Y.; Ashfold, M. N. R.; Yuan, K.; Yang, X. Exploring the Vacuum Ultraviolet Photochemistry of Astrochemically Important Triatomic Molecules. *Natl. Sci. Rev.* **2023**, *10* (8), No. nwad158, DOI: 10.1093/nsr/nwad158.
- (3) Wu, K.; Chen, J.; McBride, J. R.; Lian, T. Efficient hot-electron transfer by a plasmon-induced interfacial charge-transfer transition. *Science* **2015**, *349* (6248), 632–635.
- (4) Ye, Z. L.; Cao, T.; O'Brien, K.; Zhu, H. Y.; Yin, X. B.; Wang, Y.; Louie, S. G.; Zhang, X. Probing excitonic dark states in single-layer tungsten disulphide. *Nature* **2014**, *513* (7517), 214–218.
- (5) Kazimierczuk, T.; Fröhlich, D.; Scheel, S.; Stolz, H.; Bayer, M. Giant Rydberg excitons in the copper oxide Cu₂O. *Nature* **2014**, *514* (7522), 343–347.
- (6) Crim, F. F. Selective Excitation Studies of Unimolecular Reaction Dynamics. *Annu. Rev. Phys. Chem.* **1984**, *35* (1), 657–691, DOI: 10.1146/annurev.pc.35.100184.003301.
- (7) Patterson, H. H.; Kanan, S. M.; Omary, M. A. Luminescent homoatomic exciplexes in dicyanoargenate(I) ions doped in alkali halide crystals. 'Exciplex tuning' by site-selective excitation and variation of the dopant concentration. *Coord. Chem. Rev.* **2000**, *208* (1), 227–241.
- (8) Binnemans, K. Interpretation of europium(III) spectra. *Coord. Chem. Rev.* **2015**, *295*, 1–45.
- (9) Dang, P.; Liu, D.; Li, G.; Al Kheraif, A. A.; Lin, J. Recent Advances in Bismuth Ion-Doped Phosphor Materials: Structure Design, Tunable Photoluminescence Properties, and Application in White LEDs. *Adv. Opt. Mater.* **2020**, *8* (16), No. 1901993, DOI: 10.1002/adom.201901993.
- (10) Demchenko, A. P. Site-selective excitation: a new dimension in protein and membrane spectroscopy. *Trends Biochem. Sci.* **1988**, *13* (10), 374–377.
- (11) Chattopadhyay, A. Exploring membrane organization and dynamics by the wavelength-selective fluorescence approach. *Chem. Phys. Lipids* **2003**, *122* (1-2), 3–17, DOI: 10.1016/S0009-3084(02)00174-3.
- (12) Renger, G.; Pieper, J.; Theiss, C.; Trostmann, I.; Paulsen, H.; Renger, T.; Eichler, H. J.; Schmitt, F. J. Water soluble chlorophyll binding protein of higher plants: A most suitable model system for basic analyses of pigment–pigment and pigment–protein interactions in chlorophyll protein complexes. *J. Plant Physiol.* **2011**, *168* (12), 1462–1472.
- (13) Qian, K.; Sweeny, B. C.; Johnston-Peck, A. C.; Niu, W. X.; Graham, J. O.; DuChene, J. S.; Qiu, J. J.; Wang, Y. C.; Engelhard, M. H.; Su, D.; Stach, E. A.; Wei, W. D. Surface Plasmon-Driven Water Reduction: Gold Nanoparticle Size Matters. *J. Am. Chem. Soc.* **2014**, *136* (28), 9842–9845.
- (14) Zhang, B.; Sun, L. Artificial photosynthesis: opportunities and challenges of molecular catalysts. *Chem. Soc. Rev.* **2019**, *48* (7), 2216–2264.
- (15) Linic, S.; Christopher, P.; Ingram, D. B. Plasmonic-metal nanostructures for efficient conversion of solar to chemical energy. *Nat. Mater.* **2011**, *10* (12), 911–921.
- (16) Crabtree, G. W.; Lewis, N. S. Solar Energy Conversion. *Phys. Today* **2007**, *60* (3), 37–42.
- (17) Linsebigler, A. L.; Lu, G. Q.; Yates, J. T. Photocatalysis on TiO₂ Surfaces - Principles, Mechanisms, and Selected Results. *Chem. Rev.* **1995**, *95* (3), 735–758.
- (18) Fujishima, A.; Rao, T. N.; Tryk, D. A. Titanium Dioxide Photocatalysis. *J. Photochem. Photobiol., C* **2000**, *1* (1), 1–21.
- (19) Diebold, U. The Surface Science of Titanium Dioxide. *Surf. Sci. Rep.* **2003**, *48* (5–8), 53–229.
- (20) Thompson, T. L.; Yates, J. T. Surface Science Studies of the Photoactivation of TiO₂-New Photochemical Processes. *Chem. Rev.* **2006**, *106* (10), 4428–4453.
- (21) Fujishima, A.; Zhang, X.; Tryk, D. A. TiO₂ Photocatalysis and Related Surface Phenomena. *Surf. Sci. Rep.* **2008**, *63* (12), 515–582, DOI: 10.1016/j.surfrep.2008.10.001.
- (22) Chen, X.; Shen, S.; Guo, L.; Mao, S. S. Semiconductor-based Photocatalytic Hydrogen Generation. *Chem. Rev.* **2010**, *110* (11), 6503–6570.
- (23) Henderson, M. A. A Surface Science Perspective on Photocatalysis. *Surf. Sci. Rep.* **2011**, *66* (6–7), 185–297, DOI: 10.1016/j.surfrep.2011.01.001.
- (24) Ma, Y.; Wang, X.; Jia, Y.; Chen, X.; Han, H.; Li, C. Titanium dioxide-based nanomaterials for photocatalytic fuel generations. *Chem. Rev.* **2014**, *114* (19), 9987–10043.
- (25) Guo, Q.; Zhou, C.; Ma, Z.; Ren, Z.; Fan, H.; Yang, X. Elementary photocatalytic chemistry on TiO₂ surfaces. *Chem. Soc. Rev.* **2016**, *45* (13), 3701–3730.
- (26) Guo, Q.; Zhou, C.; Ma, Z.; Ren, Z.; Fan, H.; Yang, X. Elementary Chemical Reactions in Surface Photocatalysis. *Annu. Rev. Phys. Chem.* **2018**, *69*, 451–472.
- (27) Guo, Q.; Ma, Z.; Zhou, C.; Ren, Z.; Yang, X. Single Molecule Photocatalysis on TiO₂ Surfaces. *Chem. Rev.* **2019**, *119* (20), 11020–11041.
- (28) Guo, Q.; Zhou, C.; Ma, Z.; Yang, X. Fundamentals of TiO₂ Photocatalysis: Concepts, Mechanisms, and Challenges. *Adv. Mater.* **2019**, *31* (50), No. e1901997.
- (29) Zhu, X. Y. Electronic structure and electron dynamics at molecule–metal interfaces: implications for molecule-based electronics. *Surf. Sci. Rep.* **2004**, *56* (1-2), 1–83, DOI: 10.1016/j.surfrep.2004.09.002.
- (30) Rabitz, H.; de Vivie-Riedle, R.; Motzkus, M.; Kompa, K. Whither the Future of Controlling Quantum Phenomena? *Science* **2000**, *288* (5467), 824–828.
- (31) Henrich, V. E.; Dresselhaus, G.; Zeiger, H. J. Observation of Two-Dimensional Phases Associated with Defect States on the Surface of TiO₂. *Phys. Rev. Lett.* **1976**, *36* (22), 1335 DOI: 10.1103/PhysRevLett.36.1335.
- (32) Wang, Z.; Wen, B.; Hao, Q.; Liu, L. M.; Zhou, C.; Mao, X.; Lang, X.; Yin, W. J.; Dai, D.; Selloni, A.; Yang, X. Localized Excitation of Ti³⁺ Ions in the Photoabsorption and Photocatalytic Activity of Reduced Rutile TiO₂. *J. Am. Chem. Soc.* **2015**, *137* (28), 9146–9152, DOI: 10.1021/jacs.5b04483.
- (33) Wendt, S.; Sprunger, P. T.; Lira, E.; Madsen, G. K. H.; Li, Z. S.; Hansen, J. O.; Matthiesen, J.; Blekinge-Rasmussen, A.; Laegsgaard, E.; Hammer, B.; Besenbacher, F. The Role of Interstitial Sites in the Ti3d

- Defect State in the Band Gap of Titania. *Science* **2008**, *320* (5884), 1755–1759.
- (34) Mao, X. C.; Lang, X. F.; Wang, Z. Q.; Hao, Q. Q.; Wen, B.; Ren, Z. F.; Dai, D. X.; Zhou, C. Y.; Liu, L. M.; Yang, X. M. Band-Gap States of TiO₂(110): Major Contribution from Surface Defects. *J. Phys. Chem. Lett.* **2013**, *4* (22), 3839–3844.
- (35) Minato, T.; Sainoo, Y.; Kim, Y.; Kato, H. S.; Aika, K.; Kawai, M.; Zhao, J.; Petek, H.; Huang, T.; He, W.; Wang, B.; Wang, Z.; Zhao, Y.; Yang, J. L.; Hou, J. G. The electronic structure of oxygen atom vacancy and hydroxyl impurity defects on titanium dioxide (110) surface. *J. Chem. Phys.* **2009**, *130* (12), 124502 DOI: 10.1063/1.3082408.
- (36) Di Valentin, C.; Pacchioni, G.; Selloni, A. Electronic structure of defect states in hydroxylated and reduced rutile TiO₂(110) surfaces. *Phys. Rev. Lett.* **2006**, *97* (16), No. 166803.
- (37) Zhang, Z.; Jeng, S. P.; Henrich, V. E. Cation-Ligand Hybridization for Stoichiometric and Reduced TiO₂(110) Surfaces Determined by Resonant Photoemission. *Phys. Rev. B* **1991**, *43* (14), 12004 DOI: 10.1103/PhysRevB.43.12004.
- (38) Zuo, F.; Wang, L.; Wu, T.; Zhang, Z. Y.; Borchardt, D.; Feng, P. Y. Self-Doped Ti³⁺ Enhanced Photocatalyst for Hydrogen Production under Visible Light. *J. Am. Chem. Soc.* **2010**, *132* (34), 11856–11857.
- (39) Khomenko, V. M.; Langer, K.; Rager, H.; Fett, A. Electronic absorption by Ti³⁺ ions and electron delocalization in synthetic blue rutile. *Phys. Chem. Miner.* **1998**, *25* (5), 338–346.
- (40) Wen, B.; Hao, Q.; Yin, W. J.; Zhang, L.; Wang, Z.; Wang, T.; Zhou, C.; Selloni, A.; Yang, X.; Liu, L. M. Electronic structure and photoabsorption of Ti³⁺ ions in reduced anatase and rutile TiO₂. *Phys. Chem. Chem. Phys.* **2018**, *20* (26), 17658–17665, DOI: 10.1039/C8CP02648C.
- (41) Yin, W. J.; Wen, B.; Zhou, C.; Selloni, A.; Liu, L. M. Excess electrons in reduced rutile and anatase TiO₂. *Surf. Sci. Rep.* **2018**, *73* (2), 58–82.
- (42) Zhang, Z. R.; Bondarchuk, O.; White, J. M.; Kay, B. D.; Dohnalek, Z. Imaging Adsorbate O-H Bond Cleavage: Methanol on TiO₂(110). *J. Am. Chem. Soc.* **2006**, *128* (13), 4198–4199.
- (43) Brookes, I. M.; Muryn, C. A.; Thornton, G. Imaging Water Dissociation on TiO₂(110). *Phys. Rev. Lett.* **2001**, *87* (26), 266103 DOI: 10.1103/PhysRevLett.87.266103.
- (44) Schaub, R.; Thostrup, P.; Lopez, N.; Laegsgaard, E.; Stensgaard, I.; Norskov, J. K.; Besenbacher, F. Oxygen Vacancies as Active Sites for Water Dissociation on Rutile TiO₂(110). *Phys. Rev. Lett.* **2001**, *87* (26), 266104–266107.
- (45) Dong, S.; Hu, J.; Xia, S.; Wang, B.; Wang, Z.; Wang, T.; Chen, W.; Ren, Z.; Fan, H.; Dai, D.; Cheng, J.; Yang, X.; Zhou, C. Origin of the Adsorption-State-Dependent Photoactivity of Methanol on TiO₂(110). *ACS Catal.* **2021**, *11* (5), 2620–2630.
- (46) Peng, X. X.; Zhang, R. D.; Feng, R. R.; Liu, A. A.; Zhou, C. Y.; Guo, Q.; Yang, X. M.; Jiang, Y.; Ren, Z. F. Active Species in Photocatalytic Reactions of Methanol on TiO₂(110) Identified by Surface Sum Frequency Generation Vibrational Spectroscopy. *J. Phys. Chem. C* **2019**, *123* (22), 13789–13794.
- (47) Wang, Z. T.; Deskins, N. A.; Henderson, M. A.; Lyubnitsky, I. Inhibitive influence of oxygen vacancies for photoactivity on TiO₂(110). *Phys. Rev. Lett.* **2012**, *109* (26), No. 266103.
- (48) Yim, C. M.; Pang, C. L.; Thornton, G. Oxygen Vacancy Origin of the Surface Band-Gap State of TiO₂(110). *Phys. Rev. Lett.* **2010**, *104* (3), No. 036806.
- (49) Argondizzo, A.; Cui, X.; Wang, C.; Sun, H.; Shang, H.; Zhao, J.; Petek, H. Ultrafast multiphoton pump-probe photoemission excitation pathways in rutile TiO₂(110). *Phys. Rev. B* **2015**, *91* (15), No. 155429.
- (50) Argondizzo, A.; Tan, S. J.; Petek, H. Resonant Two-Photon Photoemission from Ti 3d Defect States of TiO₂(110) Revisited. *J. Phys. Chem. C* **2016**, *120* (24), 12959–12966.
- (51) Zhang, Y.; Payne, D. T.; Pang, C. L.; Fielding, H. H.; Thornton, G. Non-Band-Gap Photoexcitation of Hydroxylated TiO₂. *J. Phys. Chem. Lett.* **2015**, *6* (17), 3391–3395, DOI: 10.1021/acs.jpcclett.5b01508.
- (52) Wang, T.; Chen, W.; Xia, S.; Ren, Z.; Dai, D.; Yang, X.; Zhou, C. Anisotropic d-d Transition in Rutile TiO₂. *J. Phys. Chem. Lett.* **2021**, *12* (43), 10515–10520.
- (53) Ren, Z. F.; Zhou, C. Y.; Ma, Z. B.; Xiao, C. L.; Mao, X. C.; Dai, D. X.; LaRue, J.; Cooper, R.; Wodtke, A. M.; Yang, X. M. A Surface Femtosecond Two-Photon Photoemission Spectrometer for Excited Electron Dynamics and Time-Dependent Photochemical Kinetics. *Chin. J. Chem. Phys.* **2010**, *23* (3), 255–261.
- (54) Muryn, C. A.; Hardman, P. J.; Crouch, J. J.; Raiker, G. N.; Thornton, G.; Law, D. S. L. Step and Point Defect Effects on TiO₂(100) Reactivity. *Surf. Sci.* **1991**, *251-252*, 747–752.
- (55) Tan, S. J.; Zhao, Y.; Zhao, J.; Wang, Z.; Ma, C. X.; Zhao, A. D.; Wang, B.; Luo, Y.; Yang, J. L.; Hou, J. G. CO₂ Dissociation Activated through Electron Attachment on the Reduced Rutile TiO₂(110)-1 × 1 Surface. *Phys. Rev. B* **2011**, *84* (15), No. 155418.
- (56) Payne, D. T.; Zhang, Y.; Pang, C. L.; Fielding, H. H.; Thornton, G. Coverage-dependent two-photon photoexcitation at the H₂O/TiO₂ interface. *Surf. Sci.* **2016**, *652*, 189–194.
- (57) Li, X. M.; Zhang, Z. M.; Henrich, V. E. Inelastic Electron Background Function for Ultraviolet Photoelectron-Spectra. *J. Electron Spectrosc. Relat. Phenom.* **1993**, *63* (3), 253–265.
- (58) Ozawa, K.; Yamamoto, S.; Yukawa, R.; Liu, R.; Emori, M.; Inoue, K.; Higuchi, T.; Sakama, H.; Mase, K.; Matsuda, I. What Determines the Lifetime of Photoexcited Carriers on TiO₂ Surfaces? *J. Phys. Chem. C* **2016**, *120* (51), 29283–29289.
- (59) Stefan, H. *Photoelectron Spectroscopy: Principles and Applications*, 3rd ed.; Springer Science & Business Media: Berlin, Heidelberg, 2003; p 662.
- (60) Da, B.; Sun, Y.; Hou, Z.; Liu, J.; Cuong, N. T.; Tsukagoshi, K.; Yoshikawa, H.; Tanuma, S.; Hu, J.; Gao, Z.; Ding, Z. Measurement of the Low-Energy Electron Inelastic Mean Free Path in Monolayer Graphene. *Phys. Rev. Appl.* **2020**, *13* (4), No. 044055, DOI: 10.1103/PhysRevApplied.13.044055.
- (61) Tao, J. G.; Batzill, M. Role of Surface Structure on the Charge Trapping in TiO₂ Photocatalysts. *J. Phys. Chem. Lett.* **2010**, *1* (21), 3200–3206, DOI: 10.1021/jz1013246.
- (62) Krüger, P.; Bourgeois, S.; Domenichini, B.; Magnan, H.; Chandresis, D.; Le Fèvre, P.; Floreano, L.; Cossaro, A.; Verdini, A.; Morgante, A. Defects at the TiO₂(100) surface probed by resonant photoelectron diffraction. *Surf. Sci.* **2007**, *601* (18), 3952–3955.
- (63) Krüger, P.; Bourgeois, S.; Domenichini, B.; Magnan, H.; Chandresis, D.; Le Fèvre, P.; Flank, A. M.; Jupille, J.; Floreano, L.; Cossaro, A.; Verdini, A.; Morgante, A. Defect States at the TiO₂(110) Surface Probed by Resonant Photoelectron Diffraction. *Phys. Rev. Lett.* **2008**, *100* (5), No. 055501.
- (64) Casonava, R.; Prabhakaran, K.; Thornton, G. Potassium Adsorption on TiO₂(100). *J. Phys.: Condens. Matter* **1991**, *3*, S91 DOI: 10.1088/0953-8984/3/S/014.
- (65) Selcuk, S.; Selloni, A. Facet-dependent trapping and dynamics of excess electrons at anatase TiO₂ surfaces and aqueous interfaces. *Nat. Mater.* **2016**, *15* (10), 1107–1112.
- (66) Wen, B.; Yin, W. J.; Selloni, A.; Liu, L. M. Defects, Adsorbates, and Photoactivity of Rutile TiO₂(110): Insight by First-Principles Calculations. *J. Phys. Chem. Lett.* **2018**, *9* (18), 5281–5287.
- (67) Yim, C. M.; Chen, J.; Zhang, Y.; Shaw, B. J.; Pang, C. L.; Grinter, D. C.; Bluhm, H.; Salmeron, M.; Muryn, C. A.; Michaelides, A.; Thornton, G. Visualization of Water-Induced Surface Segregation of Polarons on Rutile TiO₂(110). *J. Phys. Chem. Lett.* **2018**, *9* (17), 4865–4871, DOI: 10.1021/acs.jpcclett.8b01904.
- (68) Onda, K.; Li, B.; Zhao, J.; Jordan, K. D.; Yang, J.; Petek, H. Wet Electrons at the H₂O/(110) surface. *Sci.* **2005**, *308* (5725), 1154–1158, DOI: 10.1126/science.1109366.
- (69) Tan, S.; Argondizzo, A.; Ren, J.; Liu, L.; Zhao, J.; Petek, H. Plasmonic coupling at a metal/semiconductor interface. *Nat. Photonics* **2017**, *11* (12), 806–812.
- (70) Tan, S.; Liu, L.; Dai, Y.; Ren, J.; Zhao, J.; Petek, H. Ultrafast Plasmon-Enhanced Hot Electron Generation at Ag Nanocluster/Graphite Heterojunctions. *J. Am. Chem. Soc.* **2017**, *139* (17), 6160–6168.

(71) Tan, S.; Dai, Y.; Zhang, S.; Liu, L.; Zhao, J.; Petek, H. Coherent Electron Transfer at the Ag/Graphite Heterojunction Interface. *Phys. Rev. Lett.* **2018**, *120* (12), No. 126801.

(72) Bartels, L.; Meyer, G.; Rieder, K. H.; Velic, D.; Knoesel, E.; Hotzel, A.; Wolf, M.; Ertl, G. Dynamics of Electron-Induced Manipulation of Individual CO Molecules on Cu(111). *Phys. Rev. Lett.* **1998**, *80* (9), 2004 DOI: [10.1103/PhysRevLett.80.2004](https://doi.org/10.1103/PhysRevLett.80.2004).

(73) Denzler, D. N.; Frischkorn, C.; Hess, C.; Wolf, M.; Ertl, G. Electronic Excitation and Dynamic Promotion of a Surface Reaction. *Phys. Rev. Lett.* **2003**, *91* (22), No. 226102.

(74) Madey, T. E.; Ramaker, D. E.; Stockbauer, R. Characterization of Surfaces Through Electron and Photon Stimulated Desorption. *Annu. Rev. Phys. Chem.* **1984**, *35* (1), 215–240.